THE JOURNAL OF PHYSICAL CHEMISTRY C

Article

pubs.acs.org/JPCC

Coulomb Shifts upon Exciton Addition to Photoexcited PbS Colloidal Quantum Dots

Pieter Geiregat,[†,‡,§] Arjan Houtepen,[§,∥] Yolanda Justo,[‡,§] Ferdinand C. Grozema,[∥] Dries Van Thourhout,[†,‡] and Zeger Hens*[,‡,§]

[†]Photonics Research Group, [‡]Center for Nano and Biophotonics, and [§]Physics and Chemistry of Nanostructures, Ghent University, 9000 Ghent, Belgium

[∥]Optoelectronic Materials Section, TU Delft, 2628 CN, Delft, The Netherlands

ABSTRACT: Using ultrafast hyperspectral transient absorption (TA) spectroscopy, we determine the biexciton addition energies in PbS quantum dots (QDs) with different sizes when either a cold or a hot electron−hole pair is added to a QD already containing a cooled exciton. The observed dependence of this so-called biexciton addition energy on the QD diameter and the exciton energy can be rationalized by interpreting the addition energies as the result of an imbalance in the Coulomb interactions between the newly created carriers and the carriers already present in a QD. The obtained results are therefore relevant from both a fundamental and practical point of view. They provide experimental data on Coulomb interaction between charge carriers in confined semiconductors that can be compared with theoretical estimates. Moreover, understanding the way hot−cold biexciton addition energies influence the transient absorption spectrum adds a new element to the transient absorption toolbox for the optoelectronic properties of colloidal QDs.

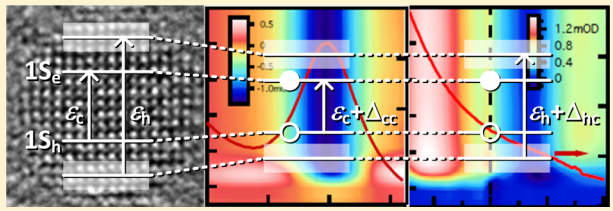

INTRODUCTION

Colloidal semiconductor nanocrystals or quantum dots (QDs) are an increasingly prominent class of low-dimensional nanomaterials that combine size-tunable electronic and optical properties with a suitability for solution-based processing. Starting from fundamental research and theoretical modeling on their unique physical properties, QDs are now applied in a variety of domains such as solar energy harvesting, photodetection, and light-emitting diodes or displays.[1−5] These applications typically rely on the linear optical properties of QDs, i.e., light absorption by unexcited QDs and light emission by radiative recombination in excited QDs. On the other hand, various studies have shown that the spectral and time-dependent properties of excited QDs can strongly enhance the performance of QD-based devices in the above mention applications or enable QDs to be used in completely different applications. Quantum dots excited with photons having energies exceeding twice that of the QD bandgap transition can, for example, dissipate their excess energy by forming biexcitons in a process called multiple exciton generation (MEG) that can considerably enhance the short circuit current of single junction, QD-based solar cells.[2,6−8] Controlling the recombination rate of biexcitons by nonradiative Auger processes allowed for the formation of blinking-free QDs and facilitated the formation of QD-based lasers.[9,10] Moreover, it was proven that excited QDs exhibit a broadband and ultrafast photoinduced absorption related to intraband transitions of either the excited electron or hole, which could be used for optical modulation.[11,12]

A ubiquitous property of excited QDs in this respect is the shift of their absorbance spectrum relative to that of unexcited QDs. These spectral shifts are typically attributed to an imbalance in the mutual electron−electron, electron−hole, and hole−hole Coulomb interactions upon addition of an exciton to an already excited QD. In the case of core/shell heteronanostructures with a staggered band alignment, for example, repulsive biexciton interactions were used to achieve single exciton gain,[13] which is otherwise unattainable when using the QD band gap transition for stimulated emission. From a more practical point of view, spectral shifts complicate the interpretation of transient absorption spectra. When present, variations of the absorbance of a QD ensemble at a given wavelength after pulsed photoexcitation do not simply reflect state-filling or photoinduced absorption, and a detailed analysis of the full transient absorption spectrum is needed.[14,15]

In spite of the importance of spectral shifts upon exciton addition for the interpretation of transient absorption spectra and the possibility to use them for tweaking QD properties, few studies have systematically addressed the properties of these shifts. Especially the effect of Coulomb interactions on high-energy transitions remains an unexplored field, although the high-energy transient absorption of near-infrared quantum dots for example is extremely important for studying the dynamical properties of hot carriers relevant for multiple-exciton generation[2,16] or carrier extraction in photovoltaic cells or

Received: June 4, 2014
Revised: August 25, 2014
Published: August 26, 2014

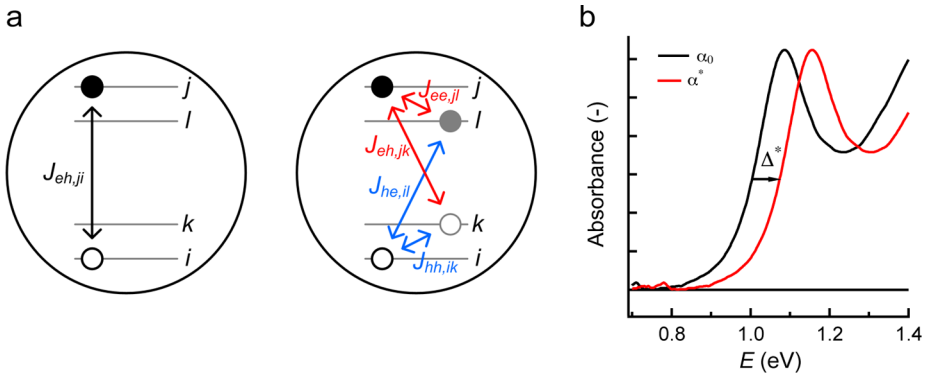

Figure 1. (a) Scheme depicting (left) electron–hole Coulomb interaction upon creation of an electron–hole pair (j, i) in an unexcited quantum dot and (right) additional Coulomb interaction terms upon creation of the same electron–hole pair (j, i) in a quantum dot already containing an electron–hole pair (l, k). (b) Representation of an absorption spectrum α_0 and its counterpart α^*, shifted by an energy difference Δ^*.

photodetectors.[17] A possible complication in this respect is the fact that a proper evaluation of spectral shifts requires the recording of the transient spectrum over a sufficiently broad wavelength range with high spectral resolution. Initial attempts by Trinh et al.[14] were conducted on PbSe QDs, but it is only recently that full broadband transient absorption studies have been reported for near-infrared absorbing QDs.[6,15,18] These however focus mostly on near-infrared probing for multiple exciton generation and, as such, do not give a detailed account of exciton addition energies.

Here, we report on a comprehensive study of spectral shifts Δ upon (multiple) exciton addition to photoexcited PbS quantum dots using transient absorption spectroscopy with white light probing. We focus first on the addition of an exciton resonant with the bandgap transition, i.e., a so-called *cold* exciton, where the spectral shift Δ_{cc} between two cold excitons is obtained by fitting the transient absorbance to a model function containing Δ_{cc} as an adjustable parameter. The ensuing biexciton addition energy is negative, with a magnitude that goes down with increasing quantum dot diameter. Next, we show that upon creation of a high energy electron–hole pair, i.e., a so-called *hot* electron–hole pair, the interaction with cold excitons already present also results in a spectral red-shift. As was pointed out by different authors, a hot electron–hole pair has not yet condensed into an exciton,[19,20] hence the wording hot electron–hole pair instead of hot exciton. The corresponding hot–cold biexciton addition energy Δ_{hc} is largely independent of the excitation energy and scales proportionally to the number of cold excitons present. The magnitude of Δ_{hc} decreases with increasing quantum dot diameter and systematically exceeds the magnitude of Δ_{cc}. On the other hand, no significant spectral shifts are measured upon addition of a hot electron–hole pair to quantum dots already containing hot electron–hole pairs. Hence, we determine that biexciton shifts increase as $\Delta_{hc} > \Delta_{cc} \gg \Delta_{hh}$. We discuss these exciton addition energies and their relative magnitude in terms of an imbalance of the electron–electron, hole–hole, and electron–hole Coulomb interactions between the newly added charge carriers and the carriers already present in the quantum dot.

CONCEPTS

Exciton Addition Energies and Coulomb Shifts. In a single electron picture, photon absorption can transfer an electron from an initial state i to a final state j of a quantum dot, where the photon energy matches the energy differency $\Delta\epsilon_{0,ij}$ given by

$$\Delta\epsilon_{0,ij} = \epsilon_{e,j} + \epsilon_{h,i} - J_{eh,ji} \quad (1)$$

Here, the subscript 0 indicates that the photon is absorbed by an unexcited QD, while $\epsilon_{e,j}$ and $\epsilon_{h,i}$ denote the electron and hole energy level, respectively—counted as positive numbers starting from the uppermost valence-band level—and $J_{eh,ji}$ is the absolute value of the Coulomb interaction energy between an electron in state j and a hole in state i (see Figure 1a). In writing eq 1, we have neglected possible contributions from configuration interaction or exchange interaction.[21,22] If the QD already contains N excitons, the transition between the same single electron states will occur at an energy difference $\Delta\epsilon_{N,ij}$ that may differ from $\Delta\epsilon_{0,ij}$ due to Coulomb interactions between the newly created electron–hole pair and the electrons and holes already present in the quantum dots. Using the different Coulomb terms as shown in Figure 1a, $\Delta\epsilon_{N,ij}$ can be written as

$$\Delta\epsilon_{N,ij} = \Delta\epsilon_{0,ij} - \sum_k (J_{eh,jk} - J_{hh,ik}) - \sum_l (J_{he,il} - J_{ee,jl}) \quad (2)$$

Here, the indices k and l label the states of all electrons and holes already present in the QD.

The concept of a spectral shift refers to the fact that the same electronic transition is observed at a different photon energy. The spectral shift $\Delta_{N,ij}$ for exciton addition to a QD already containing N excitons can therefore be defined as

$$\Delta_{N,ij} = \Delta\epsilon_{N,ij} - \Delta\epsilon_{0,ij} \quad (3)$$

Using eqs 1 and 2, $\Delta_{N,ij}$ can be written as

$$\Delta_{N,ij} = -\sum_k (J_{eh,jk} - J_{hh,ik}) - \sum_l (J_{he,il} - J_{ee,jl}) \quad (4)$$

In principle, $\Delta_{N,ij}$ depends on the electron and hole states occupied by the newly formed exciton and by the excitons already present. When analyzed using transient absorption spectroscopy, $\Delta_{N,ij}$ can therefore depend on the pump and probe photon energy and the pump–probe time delay. Assuming however that all Coulomb interaction terms are independent of the particular states occupied by the electrons and the holes already present, labeled in general as 0, eq 4 becomes

dx.doi.org/10.1021/jp505530k | J. Phys. Chem. C 2014, 118, 22284–22290

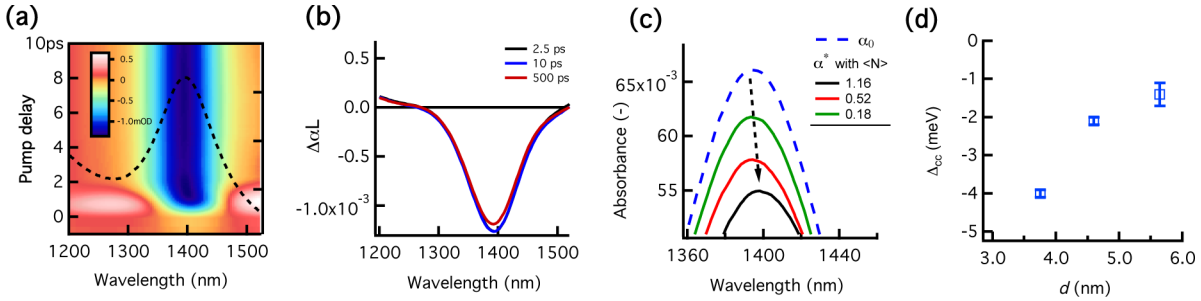

Figure 2. Low-energy (i.e., resonant) probing overview: (a) 2D time−wavelength map upon 700 nm, 180 fs photoexcitation (creating $\langle N\rangle = 0.1$) of 5.2 nm PbS QDs, plotted together with the linear absorption spectrum A_0 (dashed black line). (b) Spectral cuts at 2.5, 10, and 500 ps. (c) Nonlinear absorbance A^* (= $\Delta A + A_0$) for different fluences $\langle N\rangle$. (d) The cold−cold shift Δ_{cc} as a function of quantum dot diameter.

$$\Delta_{N,ij} = -N(J_{eh,j0} + J_{he,i0} - J_{hh,i0} - J_{ee,j0}) = N\Delta \quad (5)$$

One sees that in this case a spectral shift is obtained proportional to the number of excitons present and determined by the net difference of e−h Coulomb attraction and e−e and h−h repulsion between the newly formed electron−hole pair and the electrons and holes already present.

Determination of Spectral Shifts. In general, the absorption spectrum α^* of an ensemble of quantum dots after photoexcitation is the weighted average of the spectra of quantum dots containing 0, 1, 2, etc., excitons. Denoting the fraction of quantum dots containing N excitons by x_N, we have[14]

$$\alpha^*(\epsilon, t) = \sum_N x_N(t)\alpha_N(\epsilon, t) \quad (6)$$

With t denoting the time delay after the pump pulse, eq 6 explicitly takes the time dependence of the fractions x_i and the absorption spectra α_i into account, where the former can change due to exciton recombination while, e.g., exciton cooling can affect the latter. Spectral shifts are one of the parameters that determine the difference between α_N and α_0, and they can be determined by fitting the spectrum α^* to eq 6 while using parametrized expressions for each spectrum α_N.

A more direct determination of spectral shifts is possible when the only difference between α^* and the spectrum $\alpha_0(\epsilon)$ before excitation is a spectral shift by an energy Δ^*. In that case, one has (see Figure 1b)

$$\alpha^*(\epsilon) = \alpha_0(\epsilon - \Delta^*)$$

For sufficiently small spectral shifts, Δ^* can thus be calculated as

$$\Delta^*(\epsilon) = \frac{\alpha_0(\epsilon) - \alpha^*(\epsilon)}{d\alpha_0(\epsilon)/d\epsilon} \quad (7)$$

Using eq 6 and writing the spectral shift between the absorption spectrum α_N and α_0 as Δ_N, the spectrum α^* can be expressed as

$$\alpha^*(\epsilon) = \sum_N \left(\alpha_0(\epsilon) - \frac{d\alpha_0}{d\epsilon}\Delta_N\right)x_N$$

Entering this expression in eq 7, it thus follows that the overall spectral shift Δ^* is obtained as the weighted average of the shifts Δ_N:

$$\Delta^* = \sum_i \Delta_N x_N \quad (8)$$

When Δ_N is proportional to N (see eq 5), we obtain the result that Δ^* is proportional to the average number of excitons per QD $\langle N\rangle$:

$$\Delta^* = \langle N\rangle\Delta \quad (9)$$

EXPERIMENTAL SECTION

Oleylamine (OLA)-capped PbS QDs were synthesized using the procedure described by Cademartiri et al.[23] and modified by Moreels et al.[24] After synthesis, the OLA ligand shell is substituted by oleic acid (OA). This is done by first precipitating the QDs from the reaction mixture by addition of ethanol and redispersing the QD pellet obtained after centrifugation in 10 mL of toluene and 1.5 mL of oleic acid. After precipitation with ethanol and centrifugation, the QDs are resuspended in toluene and the exchange is repeated.

Samples were excited using 180 fs pump pulses at 700 nm, created from the 1028 nm fundamental (Pharos SP, 6 W, Light Conversion) through nonlinear frequency mixing in an OPA (Orpheus, Light Conversion). Probe pulses were generated in a sapphire crystal using the 1028 nm fundamental. The pulses were delayed relative to the pump using a delay stage with maximum delay of 2.5 ns (Helios spectrometer, Ultrafast Systems). The probe spectrum in our experiments covers the vis−NIR window from 550 up to 1600 nm. PbS quantum dots were dispersed in an optically transparent solvent (tetrachloroethylene) to achieve optical densities of 0.1 at the first exciton transition, and samples were stirred during all measurements. The average number of absorbed photons (or equivalently created excitons) $\langle N\rangle$ can be calculated from the photon flux J_{ph}, the cuvette length L, and the nanocrystal absorption cross section at the pump wavelength σ_{700}: $\langle N\rangle = J_{ph} \times \sigma_{700} \times [(1 - e^{-\alpha_{0,700}L})/\alpha_{0,700}L]$. Assuming Poissonian statistics,[25] one can write the probability to have N excitons in a nanocrystal as $P(N) = e^{-\langle N\rangle}\langle N\rangle^N/N!$.

RESULTS AND DISCUSSION

Near-Bandgap Probing. Figure 2a shows the linear absorbance spectrum A_0 of a dispersion of 5.2 nm PbS QDs, together with the 2D transient absorbance (TA) image ΔA in the wavelength range 1200−1520 nm (1.03−0.81 eV), recorded following a 180 fs optical pump pulse that creates on average 0.1 excitons per QD. At wavelengths around the band gap transition of 1400 nm (0.88 eV), a reduced absorption is observed due to the filling of the highest valence-band and lowest conduction-band states by the cooled exciton. Apart from a slight reduction in intensity, the transient absorption shows little variation in the time range 2.5−500 ps

dx.doi.org/10.1021/jp505530k | J. Phys. Chem. C 2014, 118, 22284−22290

(see Figure 2b), which is much shorter than the single exciton lifetime.[26] In Figure 2c, the nonlinear absorbance $A^* = A_0 + \Delta A$ recorded 500 ps after the pump pulse is plotted for different pump fluences as characterized by the average number of excitons $\langle N \rangle$. A^* decreases with increasing $\langle N \rangle$ due to more extensive state filling, and its maximum shows a progressive red-shift relative to the maximum of A_0 when the pump fluence is raised.

After a time delay of 500 ps, all multiexcitons initially present after the pump pulse have decayed by Auger recombination ,and only unexcited and singly excited quantum dots remain. Figure 2c therefore indicates that the addition energy of a cold exciton, i.e., resonant with the bandgap, to a quantum dot already containing a cold exciton is negative. To quantify this so-called cold−cold biexciton addition energy Δ_{cc}, we write the nonlinear absorbance A^* according to eq 6 as a function of the average exciton number at time zero $\langle N \rangle$:

$$A^* = x_0 A_0 + x_1 A_1 = e^{-\langle N \rangle} A_0(\epsilon) + [1 - e^{-\langle N \rangle}] \times \left[\frac{3}{4} A_0(\epsilon - \Delta_{cc}) + A_{IB} \right] \quad (10)$$

Here, we have used the fact that the presence of a cold exciton will reduce the absorption cross section of the bandgap transition by 1/4 since PbS quantum dots have 8-fold degenerate band edge states. Moreover, the A_1 spectrum is shifted in energy by an amount Δ_{cc}, and we have introduced an energy independent term A_{IB} to describe photoinduced absorption in excited quantum dots due to intraband transitions.[11] For PbS quantum dots with three different sizes, we have fitted the above model to the transient absorption spectra, keeping A_{IB} fixed at 5% of A_0 in line with the values reported for PbSe QDs in ref 11. Using three different average fluences per size (shown in Figure 2c for a 5.2 nm QD), we can obtain an average Δ_{cc} and a standard deviation on that value. As shown in Figure 2d, the resulting spectral shifts Δ_{cc} range from −4.0 to −1.4 meV for 3.75 to 5.6 nm PbS quantum dots. Moreover, since the standard deviation on the obtained shifts—indicated by the error bars in Figure 2d—are small, these values show little dependence, if any, on the pump fluence.

In principle, it should be possible to derive the addition energy of a cold exciton to a quantum dot containing a hot electron−hole pair from the transient absorbance spectrum in the first picoseconds after photoexcitation, i.e., before exciton cooling. However, this cold−hot biexciton addition energy Δ_{ch} is difficult to evaluate reliably since hot electron−hole pairs impose multiple effects on the band edge transition apart from regular energy shifts due to Coulomb type interactions, mainly due to the fact that the pair has not yet formed an excitonic state. It has been argued that this transient charge state induces a transient dipole moment, thus breaking the symmetry of the spherical quantum dots and allowing symmetry-forbidden dipole transition (such as S−P) to gain oscillator strength or broaden up. Other reports[11] pointed out that hot carriers showed increased intraband absorption, giving an additional transient component to ΔA at early times which is dependent on energy. Since this makes that no reliable parametrization of any A_N can be put forward, we refrain from determining Δ_{ch} using a fitting procedure.

Above Bandgap Probing. Figure 3a shows the linear absorbance spectrum of a dispersion of 3.75 nm PbS QDs, together with the transient absorbance spectrum in the wavelength range 550−900 nm (2.25−1.38 eV), recorded following a 180 fs optical pump pulse that creates on average 0.1 excitons per QD. Clearly the differential absorbance is positive. This implies that excited quantum dots absorb light more strongly than unexcited quantum dots at photon energies corresponding to 1.6−2.4 times the bandgap transition energy. This photoinduced absorption clearly depends on the probe-photon wavelength but shows only little change, if any, as a function of the pump−probe delay.

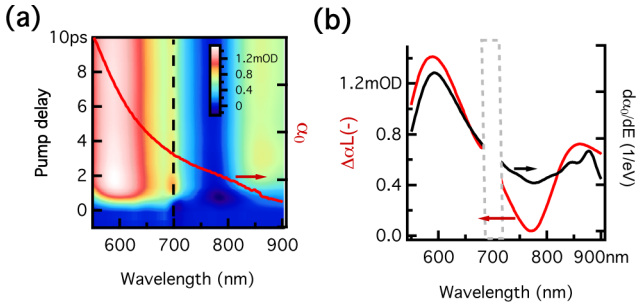

Figure 3. High-energy probing overview: (a) 2D time−wavelength map upon 700 nm, 180 fs photoexcitation (dashed vertical line) (creating $\langle N \rangle = 0.1$) of 3.75 nm PbS QDs, plotted together with the linear absorption spectrum α_0. (b) Spectral cut at 2.5 ps from (a) plotted together with $d\alpha_0/dE$ in the wavelength range of 550−900 nm.

Figure 3b depicts a spectral cut of the TA spectrum taken at 2.5 ps, together with the derivative $d\alpha_0/d\epsilon$. It follows that at photon energies at around 2.1 eV (600 nm), where the photoinduced absorption is largest, also $d\alpha_0/d\epsilon$ peaks, whereas at wavelengths around 1.6 eV (750 nm), both the photoinduced absorption and $d\alpha_0/d\epsilon$ attain a minimum value. Referring to eq 7, this suggests that the photoinduced absorption at these high photon energies results from a wavelength-independent spectral shift. Using this equation to calculate this presumed spectral shift Δ^* from the experimental TA spectrum after 2.5 ps, i.e., after the excitons created by the pump pulse have cooled to the band edges, we indeed find a largely constant, negative shift between photon energies of 550 and 700 nm (see Figure 4a). Moreover, by increasing the pump fluence, it follows that the shift Δ^* thus calculated changes proportionally to the average number of excitons $\langle N \rangle$ per QD (see Figure 4b). In this respect, Δ^* has all the properties expected for a true spectral shift according to the simple model expressed by eq 9. We therefore tentatively link the slope of the Δ^* vs $\langle N \rangle$ curve—which amounts to -4.7 ± 0.2 meV—to the net biexciton Coulomb interaction Δ as introduced in eq 5 between the hot electron−hole pair created by the probe pulse and a cold exciton resulting from the pump pulse. We will refer to this number as Δ_{hc}, i.e., the hot−cold exciton addition energy, where the observation that $\Delta_{hc} < 0$ points toward biexciton attraction.

Further confirmation of the interpretation of the photoinduced absorption as a spectral shift resulting from a nonzero exciton addition energy follows from the time dependence of Δ^*. As can be seen in Figure 4c, the photoinduced absorption decreases within the first 100 ps after photoexcitation to a steady background value once $\langle N \rangle$ is equal to or higher than 0.7. This is the typical lifetime of multiexcitons that recombine via nonradiative Auger processes, which indicates that the time dependence of Δ^* follows that of $\langle N \rangle$. Moreover, when the pump fluence is increased such that $\langle N \rangle \approx 6$ right after the pump pulse, Δ^* attains a value of −4.6 meV after 500 ps (see

dx.doi.org/10.1021/jp505530k | J. Phys. Chem. C 2014, 118, 22284−22290

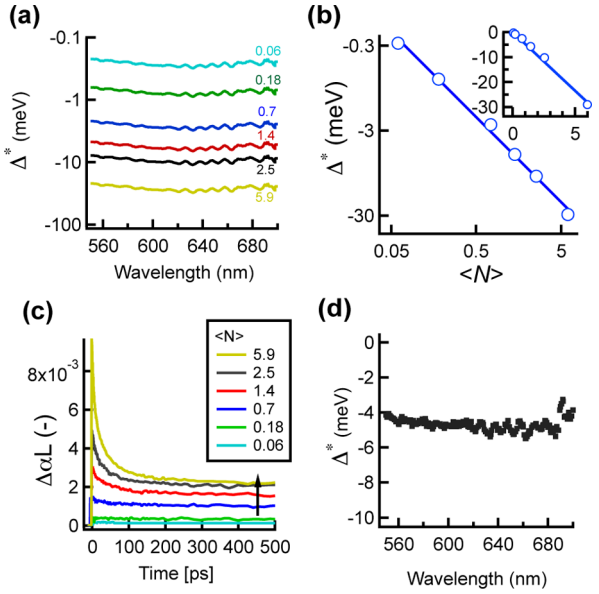

Figure 4. Analysis of 3.75 nm PbS quantum dots. (a) Spectrum of the energy shift (on a logarithmic scale) Δ* after 2.5 ps calculated from eq 7 for different average occupations ⟨*N*⟩. (b) Same energy shift at 580 nm, showing a linear dependence on ⟨*N*⟩. Inset shows the same fit on a linear scale for ⟨*N*⟩. (c) Time dependence of TA signal at 580 nm for different fluences. (d) Shift calculated from Δα at 500 ps under high fluence ⟨*N*⟩ = 5.9 such that $P(N\geq1) = 1$.

Figure 4d), a number agreeing with the spectral shift Δ attributed before to the hot−cold biexciton addition. Since almost all QDs contain a single exciton for this combination of pump intensity and pump−probe delay, this result confirms the consistency of the interpretation put forward.

In Figure 5, we represent the spectral shift Δ* for a sample of 3.75 nm PbS QDs after a 700 nm pump pulse that creates on

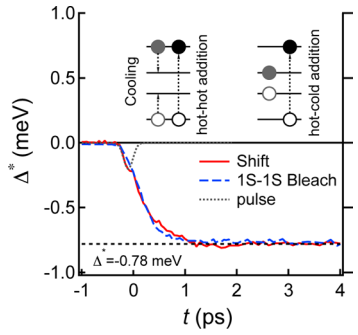

Figure 5. Representation of (solid red line) spectral shift at 580 nm during carrier cooling upon 700 nm photoexcitation and (dashed blue line) the (rescaled) bleach at the 1S−1S band gap transition of 3.75 nm PbS QDs. The fluence was chosen as to create 0.18 excitons on average, which is sufficiently low to avoid any influence of multiexcitons. As indicated by the dotted black line, the spectral shift reaches a value of −0.78 meV within ≈2 ps after photoexcitation. The dotted gray line depicts the 180 fs pump pulse.

average 0.18 excitons per QD. It follows that Δ* levels off at a value of −0.78 meV within 2 ps after the pump pulse. In line with Figure 4, this value corresponds to $\approx0.17\Delta_{hc}$, such that it can indeed be attributed to the hot−cold biexciton interaction. On the other hand, within the first picosecond after the pump pulse, the absolute value of Δ* gradually increases from naught to this final value. At these early stages, the exciton created by the pump pulse has not yet relaxed to the band edges, a conclusion confirmed by the gradual increase of the bleach of the band gap transition within the same time span (see Figure 5, blue trace). This means that the time evolution of Δ* reflects the evolution of the biexciton addition energy from a hot−hot to a hot−cold combination. As such, we could estimate an upper limit to the hot−hot interaction from a deconvolution with the 180 fs pump pulse creating the hot excitation. An example is shown in Figure 5 (dotted line), yielding a Δ_{hh} of 0.2 meV as upper limit, which is 4 times smaller than the corresponding hot−cold shift. We therefore conclude that the hot−hot biexciton interaction Δ_{hh} is small as compared to Δ_{hc}.

Figure 6 summarizes Δ_{hc} as determined for PbS quantum dots of different sizes. One sees that especially for the smallest

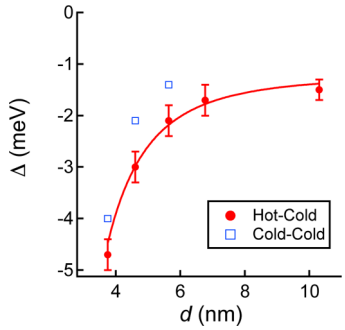

Figure 6. Different interaction energies for varying PbS quantum dot diameter *d*: The hot−cold biexciton interaction energy Δ_{hc} and the cold−cold Δ_{cc}. A $1/d^3$ dependence is fit to Δ_{hc}, indicative of an expected Coulomb type size dependence.

QDs studied, i.e., 3.75−5.65 nm, Δ_{hc} decreases quickly with increasing diameter. For the larger QDs, it drops to values in the range −1.5 to −1 meV. As compared to Δ_{hc}, the exciton addition energies Δ_{cc} as determined previously are smaller by 15−35%.

DISCUSSION

We have shown that after photoexcitation of a quantum dot ensemble using a femtosecond pump pulse, the absorbance of the sample at photon energies well above the bandgap transition increases. The change in absorbance is consistent with a spectral red-shift constant in energy, which we attribute to nonzero bi- or multiexciton addition energies. It follows that the hot−cold addition energy corresponds to the product of the biexciton addition energy Δ_{hc} and the number of cold excitons present in the quantum dot. This biexciton addition energy is a negative number—leading to the observed spectral red-shifts—with a magnitude of a few meV. It is largely independent of the actual state of the hot electron−hole pair, and its magnitude decreases with increasing quantum dot diameter. Since the initial dynamics of the spectral red-shift is identical to that of exciton cooling—raising from naught to a steady value within 1−2 ps—we conclude that the hot−hot biexciton addition energy Δ_{hh} appears to be negligible as compared to Δ_{hc}. This set of biexciton addition energies is complemented by the analysis of the spectral bleach around the band gap transition, where the cold−cold biexciton addition energy could be derived from a fit of the nonlinear absorbance to a model function that takes into account state filling, spectral shifts, and photoinduced absorption due to intraband transitions. As

dx.doi.org/10.1021/jp505530k | J. Phys. Chem. C 2014, 118, 22284−22290

compared to Δ_{hc}, Δ_{cc} is smaller by about 15−35%, while showing a similar dependence on the quantum dot diameter.

Apart from providing an interpretation of the photoinduced absorption at high photon energies, this study thus yields numbers for the hot−hot, hot−cold, and cold−cold biexcton addition energy that can be compared to the expected, based either on qualitative arguments or on more detailed numerical calculations. As argued before, nonzero biexciton addition energies are typically attributed to imbalances in Coulomb attraction and repulsion between the four charge carriers constituting the biexciton. Using the notation introduced previously, the Coulomb interaction $J_{eh,jk}$ between an electron in state j and a hole in state k can be expressed in terms of the respective single particle eigenfuctions $\psi_{c,j}$ and $\psi_{v,k}$ as[22]

$$J_{eh,jk} = \int\int \frac{|\psi_{c,j}(\mathbf{r}_1)|^2 |\psi_{v,k}(\mathbf{r}_2)|^2}{\varepsilon(\mathbf{r}_1, \mathbf{r}_2)|\mathbf{r}_1 - \mathbf{r}_2|} \, d\mathbf{r}_1 \, d\mathbf{r}_2 \quad (11)$$

Here, $\mathbf{r}_1$ and $\mathbf{r}_2$ are the position vector of the electron and the hole, respectively, whereas $\varepsilon(\mathbf{r}_1,\mathbf{r}_2)$ is the microscopic dielectric function. On the basis of eq 11, one sees from eq 4 that the biexciton addition energy will indeed get smaller with increasing quantum dot diameter, a trend in line with our observations. Moreover, exciton addition energies will reduce to zero when the wave function amplitude of all electron and hole states involved is spread identically over a quantum dot. In the same way, eq 5 indicates that with one cold electron−hole pair present biexciton addition energies will be independent of the state of the second exciton when the electron wave function amplitudes and the hole wave function amplitudes of different electron−hole pairs again have a similar distribution over the quantum dot.

Using these rules of thumb, the experimental findings on the different biexciton addition energies, i.e., Δ_{cc}, Δ_{hc}, and Δ_{hh}, can be rationalized by looking at the envelope wave function of electrons or holes at the band edges and at higher conduction or valence band states. The former are composed of small wavenumber components with an amplitude that is maximal in the center of the dot (see Figure 7). On the other hand, the latter are made up of high wavenumber components with an amplitude more equally distributed over the entire quantum dot, a distribution that will be similar for different high energy states. As a result, one expects that hot−hot biexciton addition energies should be small since all electron and hole states involved have a similar distribution of their wave function amplitude over the quantum dot. Hot−cold biexciton addition energies, on the other hand can be considerably larger, yet given the similar spreading of high energy electron and high energy hole states over the quantum dot, they will show little dependence on the particular state the hot pair is in. Finally, since the wave function amplitude of band-edge electrons and holes will be more alike than that of band-edge electrons and high energy electrons or band-edge holes and high-energy holes, the cold−cold biexciton addition energy will tend to be smaller than the hot−cold addition energy.

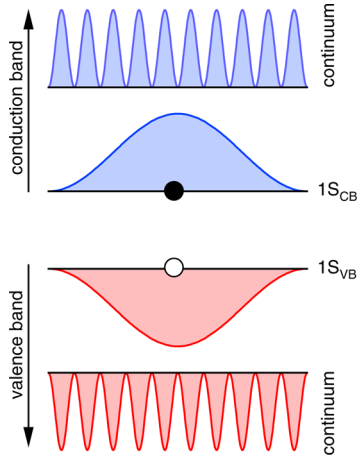

Figure 7. Schematic representation of the square of the envelope wave function of (blue) electron and (red) hole states at the band edges and in the high-energy continuum of conduction and valence band states, respectively.

The observation that the hot−cold addition energy scales as the product of the biexciton addition energy and the average number of excitons is also useful for practical purposes. Since the transient absorption spectrum of PbS quantum dots after exciton cooling is only determined by these spectral shifts in the wavelength range between 550 and 700 nm, knowledge of Δ_{hc} enables a direct determination of $\langle N \rangle$ from the differential absorbance at a single wavelength. Since $\langle N \rangle$ is a central quantity in the study of processes such as multiexciton generation, the results shown here suggest that these may be studied more directly by looking at spectral shifts in the visible part of the transient absorption spectrum rather than analyzing absorption changes around the bandgap transition.

CONCLUSIONS

We have presented an experimental study on the biexciton addition energy in colloidal PbS quantum dots for the cases where a cold exciton is added to a quantum dot already containing a cold exciton (Δ_{cc}) and a hot electron−hole pair is added to a quantum dot already containing a cold exciton (Δ_{hc}) or a hot electron−hole pair (Δ_{hh}). These exciton addition energies are derived from the transient absorption spectrum, either around the bandgap transition for cold exciton addition or at photon energies well above the bandgap for hot electron−hole pair addition. Since the transient absorbance is determined by a combination of state filling, spectral shifts, and intraband absorption in the former case, we fit the differential absorbance to a model function to derive Δ_{cc}. For hot electron−hole pair addition, on the other hand, we find that the transient absorbance in the wavelength range studied is only determined by a spectral shift. As a result, a more direct determination of Δ_{hc} and Δ_{hh} from the transient absorbance is possible. Interestingly, we find that Δ_{hc} is largely independent of the actual hot electron state and decreases strongly with increasing quantum-dot diameter. As compared to Δ_{hc}, Δ_{hh} is negligible whereas Δ_{cc} is smaller by 15−35% in the diameter range studied. These qualitative features of the different biexciton addition energies can be understood by interpreting the biexciton addition energy in terms of an imbalance of the Coulomb interactions between the newly created charge carriers and the charge carriers already present in the quantum dots.

AUTHOR INFORMATION

Corresponding Author

*E-mail: zeger.hens@ugent.be (Z.H.).

Notes

The authors declare no competing financial interest.

■ ACKNOWLEDGMENTS

The authors acknowledge Ghent University (BOF scholarship), the FWO-Vlaanderen (G.0760.12), BelSPo (IAP 7.35, photonics@be), and EU-FP7 (Strep Navolchi).

■ REFERENCES

(1) Talapin, D. V.; Lee, J.-S.; Kovalenko, M. V.; Shevchenko, E. V. Prospects of Colloidal Nanocrystals for Electronic and Optoelectronic Applications. *Chem. Rev.* **2010**, *110*, 389−458.

(2) Beard, M. C.; Luther, J. M.; Semonin, O. E.; Nozik, A. J. Third Generation Photovoltaics Based on Multiple Exciton Generation in Quantum Confined Semiconductors. *Acc. Chem. Res.* **2013**, *46*, 1252−1260.

(3) McDonald, S. A.; Konstantatos, G.; Zhang, S.; Cyr, P. W.; Klem, E. J. D.; Levina, L.; Sargent, E. H. Solution-Processed PbS Quantum Dot Infrared Photodetectors and Photovoltaics. *Nat. Mater.* **2005**, *4*, 138−42.

(4) Clifford, J. P.; Konstantatos, G.; Johnston, K. W.; Hoogland, S.; Levina, L.; Sargent, E. H. Fast, Sensitive and Spectrally Tuneable Colloidal Quantum-Dot Photodetectors. *Nat. Nanotechnol.* **2009**, *4*, 40−44.

(5) Cho, K.-S.; Lee, E. K.; Joo, W.-J.; Jang, E.; Kim, T.-H.; Lee, S. J.; Kwon, S.-J.; Han, J. Y.; Kim, B.-K.; Choi, B. L.; et al. High-Performance Crosslinked Colloidal Quantum-Dot Light-Emitting Diodes. *Nat. Photonics* **2009**, *3*, 2−6.

(6) Gdor, I.; Sachs, H.; Roitblat, A.; Strasfeld, D. B.; Bawendi, M. G.; Ruhman, S. Exploring Exciton Relaxation and Multiexciton Generation in PbSe Nanocrystals Using Hyperspectral Near-IR Probing. *ACS Nano* **2012**, *6*, 3269−3277.

(7) Aerts, M.; Suchand Sandeep, C. S.; Gao, Y.; Savenije, T. J.; Schins, J. M.; Houtepen, A. J.; Kinge, S. S.; Siebbeles, L. D. Free Charges Produced by Carrier Multiplication in Strongly-Coupled PbSe Quantum Dot Films. *Nano Lett.* **2011**, *11*, 4485−4489.

(8) Sandeep, C. S. S.; Cate, S. T.; Schins, J. M.; Savenije, T. J.; Liu, Y.; Law, M.; Kinge, S.; Houtepen, A. J.; Siebbeles, L. D. A. High Charge-Carrier Mobility Enables Exploitation of Carrier Multiplication in Quantum-Dot Films. *Nat. Commun.* **2013**, *4*, 1−6.

(9) Mahler, B.; Spinicelli, P.; Buil, S.; Quelin, X.; Hermier, J.-P.; Dubertret, B. Towards Non-Blinking Colloidal Quantum Dots. *Nat. Mater.* **2008**, *7*, 659−664.

(10) Garca-Santamara, F.; Chen, Y.; Vela, J.; Schaller, R. D.; Hollingsworth, J. A.; Klimov, V. I. Suppressed Auger Recombination in "Giant" Nanocrystals Boosts Optical Gain Performance. *Nano Lett.* **2009**, *9*, 3482−8.

(11) De Geyter, B.; Houtepen, A. J.; Carrillo, S.; Geiregat, P.; Gao, Y.; Ten Cate, S.; Schins, J. M.; Van Thourhout, D.; Delerue, C.; Siebbeles, L. D. A.; et al. Broadband and Picosecond Intraband Absorption in Lead-Based Colloidal Quantum Dots. *ACS Nano* **2012**, *6*, 6067−6074.

(12) Gao, Y.; Suchand Sandeep, C. S.; Schins, J. M.; Houtepen, A. J.; Siebbeles, L. D. A. Disorder Strongly Enhances Auger Recombination in Conductive Quantum-Dot Solids. *Nat. Commun.* **2013**, *4*, 2329.

(13) Klimov, V. I.; Ivanov, S. A.; Nanda, J.; Achermann, M.; Bezel, I.; McGuire, J. A.; Piryatinski, A. Single-Exciton Optical Gain in Semiconductor Nanocrystals. *Nature* **2007**, *447*, 441−6.

(14) Trinh, M. T.; Houtepen, A. J.; Schins, J. M.; Piris, J.; Siebbeles, L. D. A. Nature of the Second Optical Transition in PbSe Nanocrystals. *Nano Lett.* **2008**, *8*, 2112−7.

(15) Gesuele, F.; Sfeir, M. Y.; Koh, W.-K.; Murray, C. B.; Heinz, T. F.; Wong, C. W. Ultrafast Supercontinuum Spectroscopy of Carrier Multiplication and Biexcitonic Effects in Excited States of PbS Quantum Dots. *Nano Lett.* **2012**, *12*, 2658−64.

(16) Witzel, W.; Shabaev, A.; Hellberg, C.; Jacobs, V.; Efros, A. Quantum Simulation of Multiple-Exciton Generation in a Nanocrystal by a Single Photon. *Phys. Rev. Lett.* **2010**, *105*, 1−4.

(17) Tisdale, W. A.; Williams, K. J.; Timp, B. a.; Norris, D. J.; Aydil, E. S.; Zhu, X.-Y. Hot-Electron Transfer from Semiconductor Nanocrystals. *Science* **2010**, *328*, 1543−1547.

(18) Gdor, I.; Yang, C.; Yanover, D.; Sachs, H.; Lifshitz, E.; Ruhman, S. Novel Spectral Decay Dynamics of Hot Excitons in PbSe Nanocrystals: A Tunable Femtosecond PumpHy-perspectral Probe Study. *J. Phys. Chem. C* **2013**, *117*, 26342−26350.

(19) Cho, B.; Peters, W. K.; Hill, R. J.; Courtney, T. L.; Jonas, D. M. Bulklike Hot Carrier Dynamics in Lead-Sulfide Quantum Dots. *Nano Lett.* **2010**, *10*, 2498−505.

(20) Trinh, M. T.; Sfeir, M. Y.; Choi, J. J.; Owen, J. S.; Zhu, X. A Hot Electron-Hole Pair Breaks the Symmetry of a Semiconductor Quantum Dot. *Nano Lett.* **2013**, *13*, 6091−7.

(21) Franceschetti, A.; Zunger, A. Addition Energies and Quasiparticle Gap of CdSe Nanocrystals. *Appl. Phys. Lett.* **2000**, *76*, 1731.

(22) An, J. M.; Franceschetti, A.; Zunger, A. The Excitonic Exchange Splitting and Radiative Lifetime in PbSe Quantum Dots. *Nano Lett.* **2007**, *7*, 2129−2135.

(23) Cademartiri, L.; Montanari, E.; Calestani, G.; Migliori, A.; Guagliardi, A.; Ozin, G. A. Size-Dependent Extinction Coefficients of PbS Quantum Dots. *J. Am. Chem. Soc.* **2006**, *128*, 10337−46.

(24) Moreels, I.; Justo, Y.; De Geyter, B.; Haustraete, K.; Martins, J. C.; Hens, Z. Size-Tunable, Bright and Stable PbS Quantum Dots: A Surface Chemistry Study. *ACS Nano* **2011**, *5*, 2004−2012.

(25) Klimov, V. I. Quantization of Multiparticle Auger Rates in Semiconductor Quantum Dots. *Science* **2000**, *287*, 1011−1013.

(26) Justo, Y.; Geiregat, P.; Hoecke, K. V.; Vanhaecke, F.; Donega, C. D. M.; Hens, Z. Optical Properties of PbS/CdS Core/Shell Quantum Dots. *J. Phys. Chem. C* **2013**, *117*, 20171−20177.